

PCCP

Accepted Manuscript



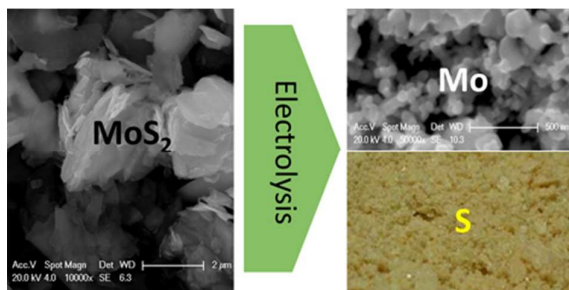
This is an *Accepted Manuscript*, which has been through the Royal Society of Chemistry peer review process and has been accepted for publication.

Accepted Manuscripts are published online shortly after acceptance, before technical editing, formatting and proof reading. Using this free service, authors can make their results available to the community, in citable form, before we publish the edited article. We will replace this *Accepted Manuscript* with the edited and formatted *Advance Article* as soon as it is available.

You can find more information about *Accepted Manuscripts* in the [Information for Authors](#).

Please note that technical editing may introduce minor changes to the text and/or graphics, which may alter content. The journal's standard [Terms & Conditions](#) and the [Ethical guidelines](#) still apply. In no event shall the Royal Society of Chemistry be held responsible for any errors or omissions in this *Accepted Manuscript* or any consequences arising from the use of any information it contains.

Table of contents



The electrolysis of solid MoS₂ to nano-Mo and elemental S in molten NaCl-KCl has been proposed and studied in detail.

Preparation of Mo Nanopowders through Electroreduction of Solid MoS₂ in Molten KCl-NaCl

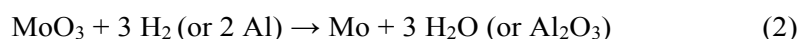
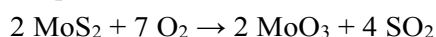
Haiping Gao^a, Mingsheng Tan^a, Liangbin Rong^a, Zhiyong Wang^a, Junjun Peng^a, Xianbo Jin^{a,*}, George Z. Chen^{a, b}

Electrolysis of MoS₂ to produce Mo nanopowders and elemental sulfur has been studied in the equimolar mixture of NaCl and KCl at 700 °C. The reduction mechanism was investigated by cyclic voltammetry (CV), potentiostatic and constant voltage electrolysis together with spectroscopic and scanning electron microscopic analyses. The reduction pathway was identified as MoS₂ → L_xMoS₂ (x ≤ 1, L = Na or K) → L₃Mo₆S₈ and LMo₃S₃ → Mo, and the last step to the formation of Mo was found to be relatively slow in kinetics. Electrolysis at a cell voltage of 2.7 V has led to a rapid reduction of MoS₂ to nodular Mo nanoparticles (50~100 nm), with the current efficiency and energy consumption being about 92 % and 2.07 kWh/ kg-Mo, respectively.

Introduction

Mo (molybdenum) and Mo based alloys have the ability to withstand extremely high temperatures and very corrosive environments, and are widely used as structural and, electronic materials, and casting moulds and containers. It is also a useful alloying additive to stainless steels for enhanced hardenability, strength, toughness, and resistance to high temperatures. Consequently, Mo containing steels account for one tenth of the total steel production of the world.¹⁻⁵ Mo is comparable to Pt in terms of anti-erosion capability to molten glass, and is used as the electrode and structural units in the glass furnace.^{3,4} Other Mo based alloys, such as MoTi(Zr), MoRe and MoW, possess high strength and high hardness at elevated temperatures. Particularly, MoRe is stable up to 2000 °C,⁶ and thus has important applications in the aerospace and engine industry. The components of Mo and Mo alloys are usually fabricated by powder metallurgy, during which, the powder of the metals were pressed to green bodies and then sintered at about 2100 °C.^{6,7}

Molybdenite (MoS₂) is the main natural source of molybdenum. The present Mo metallurgy includes two main steps as represented by reactions (1) and (2) below: (1) calcination of MoS₂ to MoO₃ in air at a temperature of 700 °C, and (2) thermal reduction of MoO₃ to the metal by hydrogen or aluminium.⁸⁻¹⁰



Such processes are extremely environment unfriendly because that the emission of SO₂ generated by reaction (1) can lead to serious acid rain.⁹⁻¹¹ On the other hand, the use of H₂ or Al is expensive. Particularly, Al is produced by electrolysis in molten fluoride salts with high energy consumption and serious CO₂ emission.

Vacuum decomposition of MoS₂ to Mo and valuable S has been suggested to be a clean alternative route, however, the process temperature is too high (>1900 °C).^{6,12} Electrolytic decomposition of MoS₂ would be preferable. This is because the theoretical decomposition voltage of MoS₂ to metallic Mo and elemental S is very low, for example, 0.57 V at 700 °C (MoS₂ → Mo + S₂ (gas), ΔG_r[⊖] = 221.034 kJ/mol). Thus, direct electrometallurgy of MoS₂ would be very energy-efficient and environmental friendly. Electrolysis of dissolved metal sulfides in molten chlorides has been attempted at about 700 °C, and while the metal deposits on the cathode, the graphite has been confirmed to be a good inert anode on which S²⁻ ions are oxidized to the S₂ gas.¹³⁻¹⁸ For example, it was proposed to produce Al by electrolysis of dissolved Al₂S₃ in molten chlorides, although there are difficulties in preparation of and handling with the anhydrous Al₂S₃. On the other hand, dissolution of these metal sulfides (such as Al₂S₃ and PbS) was often achieved by addition of the respective metal chlorides (e.g. AlCl₃ and PbCl₂) into the melt, which is challenging because of the high partial pressures of these transition metal chlorides at elevated temperatures.^{17,18}

Another electrometallurgy concept was put forward as exemplified in the preparation of Ti by electrolysis of a solid TiO₂ cathode in molten CaCl₂.¹⁹ During electrolysis, the cathode remains in solid, and it is the O²⁻ ion that leaves the cathode, diffuses through the molten salt, and then discharges to CO₂ at a graphite anode (or O₂ on an inert anode^{20,21}). This method has attracted numerous attentions for preparation of various transition metals and their alloys from their oxide precursors as reviewed recently.²² The electrolysis of solid sulfides in CaCl₂ based molten salts have also been predicted and previously investigated at 800 °C or higher temperatures.²³⁻²⁶ Similar to solid oxides, solid sulfides can be reduced to the respective solid metals, and the S²⁻ ions then transfer to the graphite anode through the molten salt, and discharge to the S₂ gas. Unfortunately, the cathodic products could be significantly contaminated by CaS²⁶ even after prolonged electrolysis, indicating the insufficient dissolution capacity of CaCl₂ for the S²⁻ ions. However, it has been demonstrated that the mixtures of KCl and NaCl possess much higher capacity for dissolution and transport of S²⁻ ions even at a relatively lower temperature (e.g. 700 °C). In this mixture, solid WS₂ has been electrolyzed to W nanopowder and element S at high speed and current efficiency against the inert graphite anode.²⁷

This paper reports our findings from direct electrolysis of solid MoS₂ in the equimolar NaCl-KCl mixture at 700 °C. The reduction mechanism has been elucidated according to results from cyclic voltammetry (CV), potentiostatic and constant voltage electrolysis. We are also motivated to find a facile process for making Mo nanopowders that would otherwise be very difficult or expensive to produce by a traditional method.

Experimental

The as-received analytical grade NaCl (351 g) and KCl (449 g) granules (99.5%, Sinopharm Chemical Reagent Co., Ltd, China) were mixed together and added into a Graphite crucible with 9.0 cm inner diameter and 23.5 cm height (99.99%, Jing Shi Ceramics Co., Ltd. Shanghai, China) which was the placed in a vertical stainless steel tube reactor under argon (99.999%, Wuhan Iron and Steel (Group) Corp., China). The temperature of the reactor was controlled by a programmable box furnace. The mixture was heated to 300 °C for 10 h to remove moisture. At a rate of 3°C min⁻¹ the temperature was raised to 700 °C for electrochemical experiments. Pre-electrolysis was carried out at 2.4 V between a nickel foil cathode and a graphite rod anode in order to remove possible redox active impurities in the melt.

Cyclic voltammograms (CVs) of solid MoS₂ (AR grade, 99%, Kemi'ou Reagent Plant, Tianjin, China) in the mixture of NaCl-KCl were recorded using a Mo metallic cavity electrode²⁷ (MCE), with the MoS₂ powder (~ 0.5 mg) as the active material filled in the through-hole cavity (0.5 mm in both diameter and depth, see inset of Figure 1a). Further, the MoS₂ powder was pressed into a cylindrical pellet (0.3 g in weight, 1.3 cm in diameter, or 1.45 g in weight, 2 cm in diameter; pressure: 4Mpa ~ 6Mpa), sintered in argon at 300 °C for about 2 h and then sandwiched between two wire meshes of molybdenum to form an assembled cathode for the constant potential (three electrode) or cell voltage (two electrode) electrolysis. A graphite rod (15 mm in diameter, 99.99%, Jingshi Ceramics Co., Ltd. Shanghai, China) was used as the counter electrode (anode) for all electrochemical tests. In voltammetric and potentiostatic experiments, the potential was controlled against a quartz sealed Ag/AgCl reference electrode as described previously.²⁸ The CVs were recorded on a computer-controlled CHI660A Electrochemical System (Shanghai Chenhua, China), while the constant potential or cell voltage electrolysis was controlled by a multichannel four-electrode potentiostat (Neware, China). After electrolysis, the cathode pellet was lifted above the melt, cooled in argon, washed with distilled water and dried under vacuum at 80 °C.

Electrolysis products were characterized by X-ray diffraction spectroscopy (XRD, X-ray 6000 with Cu K α radiation at $\lambda=1.5405$ Å, Shimadzu, Japan), and scanning electron microscope (SEM, FEI Sirion Field Emission Gun SEM system) together with energy dispersive X-ray (EDX) analysis.

Results and discussion

Figure 1 shows the CVs of Mo cavity electrode with and without the MoS₂ powder (see the inset) in the NaCl-KCl melt at 700 °C. The large reduction current at about -2.1 V on the blank MCE, labeled as c5, can be attributed to the reduction of the cations from the melt. Figure 1a presents three consecutive CVs of MoS₂ at 10 mV/s, showing clearly four reduction peaks c1, c2, c3 and c4 in the first cycle. These peaks between 0 and -2.0 V indicate the complexity of the electro-reduction of MoS₂ in the NaCl-KCl melt, but they could be hardly seen in the following cycles, indicating that the MoS₂ powder in the cavity was fully reduced to Mo after the first negative scan. To check it, the integrating charge of the four reduction currents has been calculated, which was about 1.324 C, matching very well with the theoretical charge (about 1.206 C) needed for the complete reduction of the 0.5 mg MoS₂ in the MCE. On the other hand, Figure 1a also shows two very small reoxidation peaks a2 and a1 at potentials of about -1.1 V and -0.7 V respectively, which became more noticeable in both the current and integral charge as the scan rate increased to 50 mV/s (Figure 1b). These features should have been associated to the irreversible diffusion of the S²⁻ ions out of the MCE. As a result, the amount of S²⁻ in the cavity that could be re-captured for re-oxidation was dependent on the time or scan rate.²⁷ These findings also suggest that the S²⁻ could diffuse quickly away from the MCE in the NaCl-KCl melt at 700 °C.²⁷

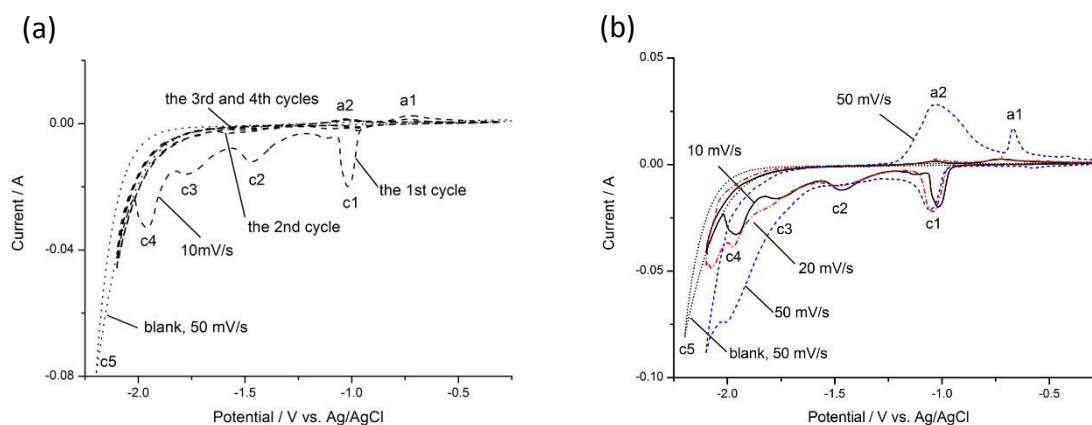


Figure 1. Cyclic voltammograms (CVs) of the Mo cavity electrodes (MCEs) loaded without (blank) and with the MoS₂ powder in equimolar NaCl-KCl mixture at 700 °C. (a) Consecutive CVs at 10 mV/s, (b) CVs at different scan rates as indicated. The insert image in (a) shows the powder loaded MCE.

MoS₂ is known to have a layered structure, and can be intercalated by Na⁺ or K⁺ ions owing to the existence of Vander Waals gaps between the covalently bound S-Mo-S sandwiches.²⁹ The reduction of MoS₂ in the NaCl-KCl melt should also undergo electrochemical intercalation of Na⁺ and/or K⁺ ions. Figure 2 shows specially four consecutive CVs of MoS₂ at 50 mV/s in the potential range from -0.6 V to -1.2 V, indicating that peaks c1 and a1 are a redox pair, which correspond most likely to the intercalation and deintercalation reactions.

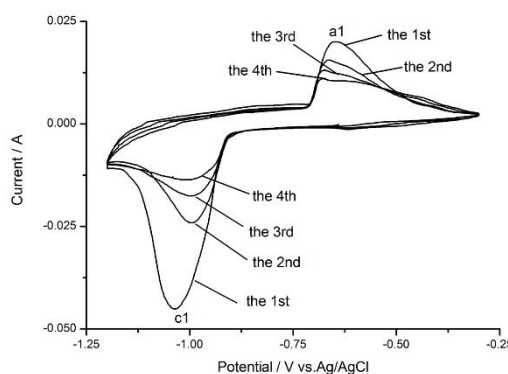


Figure 2. Consecutive CVs of the indicated cycles of the MCEs loaded with MoS₂ powder in the potential range between -0.6 and -1.2 V at 50 mV/s in the equimolar NaCl-KCl mixture at 700 °C.

In order to further understand the electro-reduction process, a series of potentiostatic electrolysis of the MoS₂ pellets were carried out at different potentials between -0.8 V and -1.8 V vs. Ag/AgCl. The studied pellet was about 0.3 g in mass, and the theoretical charge Q needed for complete reduction was about 724 C.

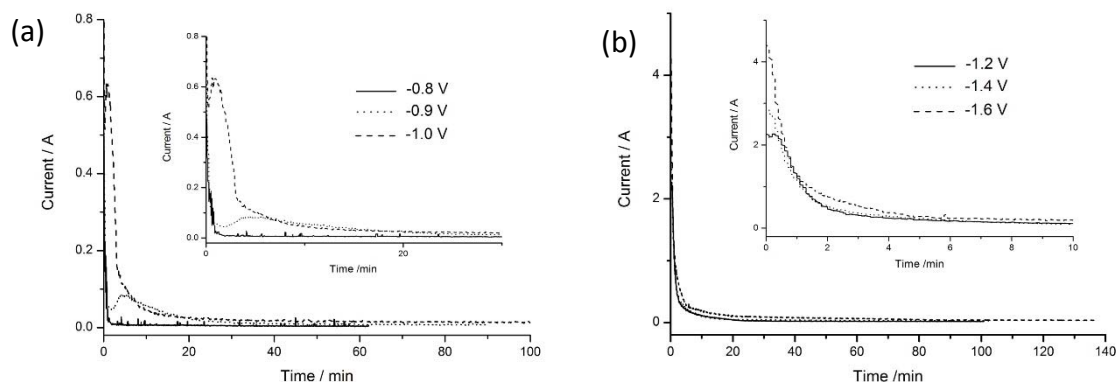


Figure 3. Typical current-time curves recorded during the potentiostatic electrolysis of MoS₂ pellets (0.3 g) at the indicated potentials (vs. Ag/AgCl) in molten NaCl-KCl (700 °C).

As shown in Figure 3a, the current responding to the suddenly imposed potential of -0.8 V displays only the charging current to the double layer, and the pellet after the electrolysis was still MoS₂ as indicated by the XRD analysis (Figure 4). The reduction of MoS₂ took place at potentials more negative than -0.9 V (versus Ag/AgCl). After the double layer charging, the reduction current climbed first, and then decreased, forming a reduction current peak. This feature has been commonly observed in electrolysis of solid oxide pellets, and rationalized by the dynamic metal/metal oxide/electrolyte three phase interlines (3PIs) theory.^{30,31} Similar to an oxide pellet cathode, the electronic contacts between the Mo meshes and MoS₂ pellet were limited, but considering that MoS₂ is a semiconductor, the initial reduction may occur in the neighbouring zone around each 3PI (metal/MoS₂/electrolyte). The transverse development of such reaction zones on the pellet surface may still cause an initial increase of the cathodic current, which then decreases due to the increasing ohmic and mass transfer polarisations of the reduction in the depth direction. However, at a very negative potential, the development of the reaction zones on the surface should be very quick. In such a case, the ohmic resistance in the MoS₂ cathode could be overcome, allowing the simultaneous occurrence of charge transfer reactions at the whole metal sulfide/NaCl-KCl interface. Consequently, the current peak would become imperceptible as shown by the current-time curves of -1.4 V and -1.6 V in Figure 3b.

In line with reduction peak c1 on the CVs, the reduction current at -0.9 V (Figure 3a) can be attributed to the formation of L_xMoS₂ ($x \leq 1$, L = Na or K) as a result of electrochemical intercalation of Na⁺ and/or K⁺.²⁹ The integral cathodic charge of about 70 C for the 0.3 g MoS₂ pellet corresponds to $x \approx 0.4$ in L_xMoS₂. The x value should be potential dependent before it reaches 1: the more negative is the potential, the larger is the x value. The cathodic charge at -1.0 V increased to about 198 C, which can be compared with the theoretical charge (about 180 C) needed for the formation of LMoS₂. Thus it can be confirmed that the cathodic peak c1 on the CVs (Figure 1 and 2) is mainly due to the electrochemical insertion reaction.

However, the XRD patterns of the products obtained at -0.9 V (Figure 4a) and -1.0 V (Figure 4b) both showed the feature (002) peak of MoS₂ at 14.4°, except that the peak became weaker and broader. This might be due to that MoS₂ had undergone formation of L_xMoS₂ as a result of electrochemical intercalation of Na⁺ and/or K⁺ during electrolysis followed by deintercalation during the post-electrolysis treatments in

water and air.²⁹ To verify this thought, a 1.45g pellet was electrolysed at -0.95 V for 2 h, and the product was quickly washed in water for the XRD measurement. Clearly, the freshly washed product was mainly $L_x\text{MoS}_2$ with x close to 1 as evidenced by the shift of the (002) peak to about 9.5° due to lattice expansion in MoS_2 . A small peak at 14.4° was also observed, indicating that partial reaction between $L_x\text{MoS}_2$ and water to form MoS_2 . However, after aging in air, the 9.5° peak decreased significantly, accompanied by an increase of the 14.4° peak, suggesting the occurrence of deintercalation of L from the $L_x\text{MoS}_2$ phase in air.

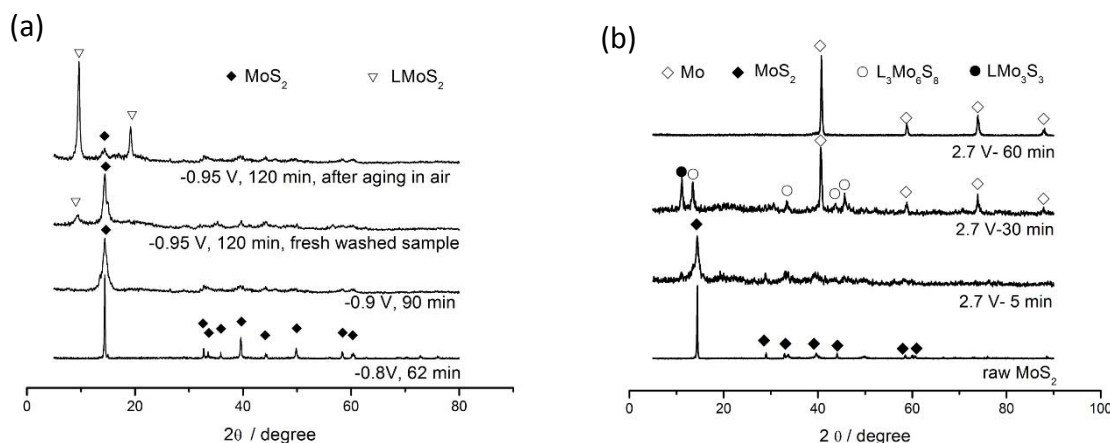


Figure 4. XRD patterns of the products from potentiostatic electrolysis of the MoS_2 pellets at the indicated potentials for different times (700 °C NaCl-KCl melt). Each MoS_2 pellet was 0.3 g except the -0.95 V one, which was 1.45 g.

Small amounts of $L_3\text{Mo}_6\text{S}_8$ and LMo_3S_3 were found in the products from electrolysis at -1.0 V as indicated by the XRD patterns. These phases became dominant at potentials of -1.2 ~ -1.4 V, and the featured XRD peak at about 14.4° disappeared, indicating the complete conversion of the MoS_2 and LMoS_2 to $L_3\text{Mo}_6\text{S}_8$ and LMo_3S_3 . At the same time, the reduction charges at -1.2 and -1.4 V (Figure 3b, ~ 385 and 410 C respectively) were slightly higher than a half of that (724 C) needed for the complete reduction of MoS_2 to Mo. According to these results, the current peak c2 on the CVs in Figure 1a and 1b can be ascribed to the reduction of LMoS_2 to $L_3\text{Mo}_6\text{S}_8$ and LMo_3S_3 . It is worth noting that the LMo_3S_3 phase also has a hexagonal structure like LMoS_2 and MoS_2 , and the $L_3\text{Mo}_6\text{S}_8$ has the same rhombohedral structure as Mo_3S_4 but with lattice expansion. Therefore, both LMo_3S_3 and $L_3\text{Mo}_6\text{S}_8$ may release L^+ ions upon oxidation. Indeed, they reacted with water during washing with hydrogen gas generated.

As the CVs in Figure 1a and 1b show two other current peaks at about -1.77 V (c3) and -1.96 V (c4), it is surprising that the electrolytic product at -1.6 V was almost pure Mo as identified by XRD. Meanwhile, the calculated reduction charge (~ 752 C) according to the current-time plot in Figure 3b indicated as well the complete reduction of the MoS_2 pellet to Mo. Such a mismatch indicates that the reduction of $L_3\text{Mo}_6\text{S}_8$ and LMo_3S_3 to Mo may occur at much more positive potentials thermodynamically, but may suffer seriously from slow kinetics. To confirm this assumption, CVs were recorded on the MoS_2 loaded MCE after constant potential electrolysis at -1.4 V and -1.6 V, respectively. In Figure 5, it can be seen that after the potentiostatic electrolysis at -1.4 V for 600 s, there was still a large cathodic current at potentials more negative than -1.6 V. On the contrary, no reduction peak was seen on the CV after electrolysis

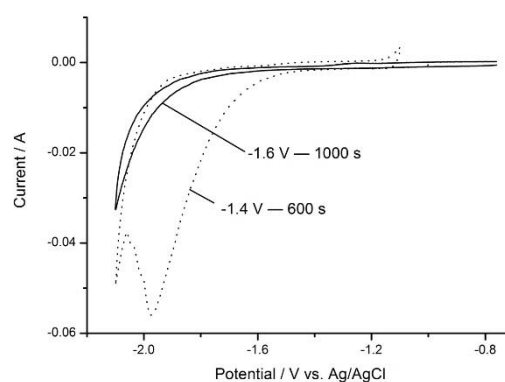
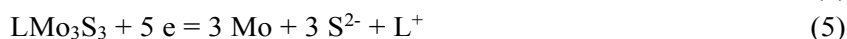
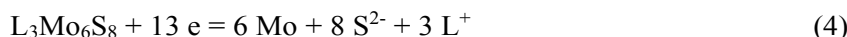
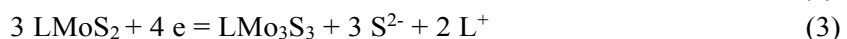
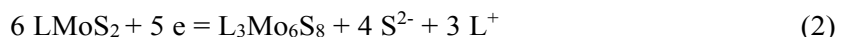
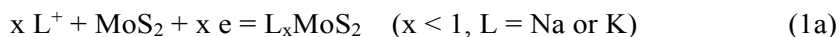


Figure 5. CVs of the MCEs loaded with MoS_2 recorded after holding the potential at -1.4 V for 600 s and -1.6 V for 1000 s respectively (50 mV/s, 700 °C, NaCl-KCl melt).

at -1.6 V for 1000 s, indicating again the thermodynamic instability of the species for the c3 and c4 peaks at -1.6 V.

Based on these findings, the mechanism for the electro-reduction of MoS₂ in the NaCl-KCl melts might be represented by reactions (1) to (5) below,



The morphologies of the electrolysis products at different potentials were revealed by SEM and are presented in Figure 6. The inserted EDX spectra indicate the initial inclusion of the Na and K elements in the reduction products at potentials between -0.9 V and -1.4 V, and the release of these two element later upon formation of Mo, which supports reactions (1~5).

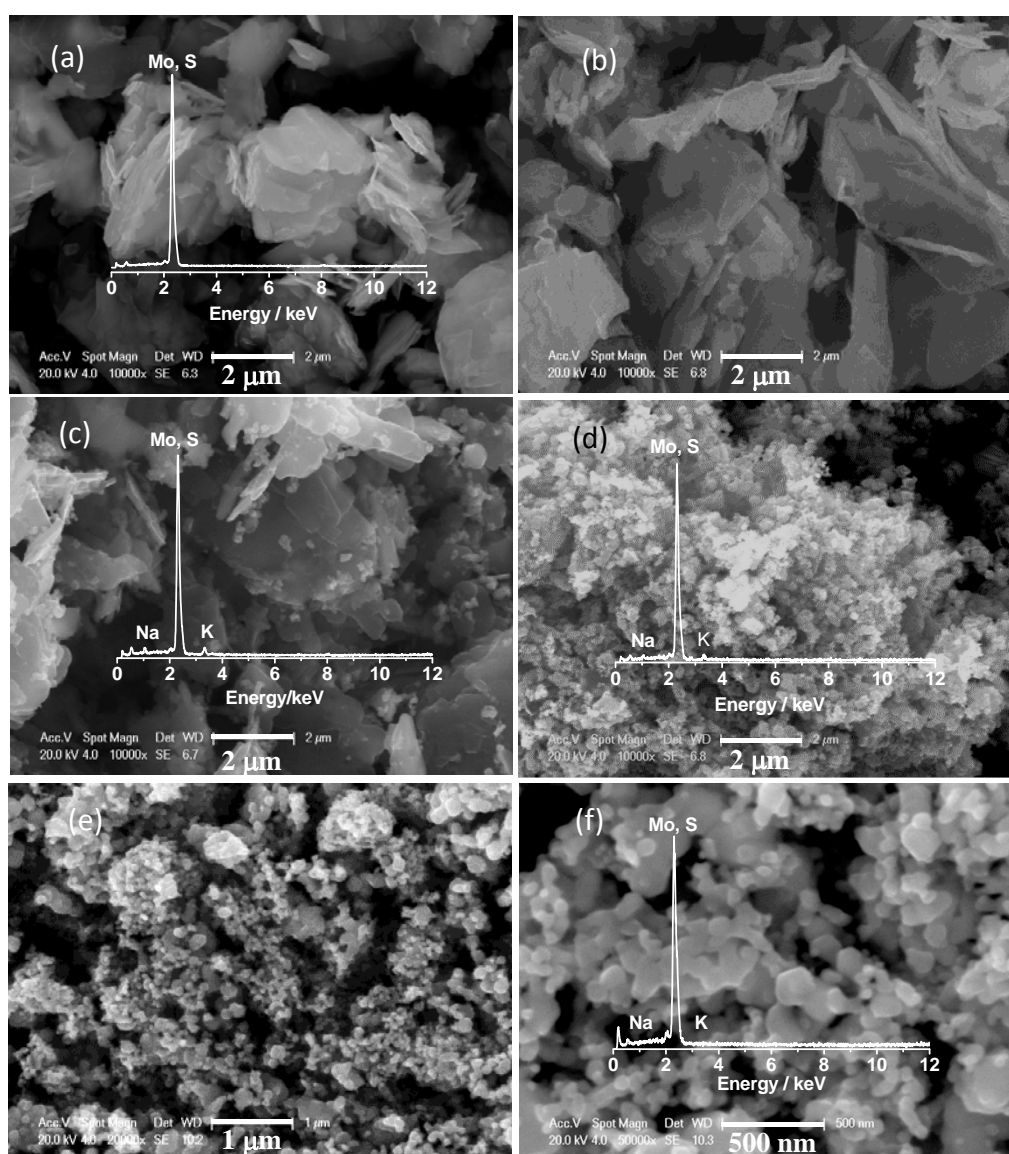


Figure 6. Typical SEM images and EDX spectra of (a) the raw MoS₂ powder, and (b-f) the products from electrolysis of MoS₂ pellets under different conditions: (b) -0.8 V, 62 min; (c) -0.9 V, 90 min; (d) -1.4 V, 103 min; (e) -1.6 V, 130 min; (f) 2.7 V, 2 h. For (b-e), potentiostatic electrolysis, 0.3 g MoS₂; for (f): constant cell voltage electrolysis, 1.45 g MoS₂. In all experiments, electrolysis was carried out at 700 °C in NaCl-KCl.

The original MoS₂ powder (Figure 6a) had an average particle size of about 2~3 μm, consisting of mainly stacks of sheets. The grain sizes increased after electrolysis at -0.8 V, likely due to sintering at 700 °C (Figure 6b). The electrolysis product (Figure 6c) at -0.9 V consisted of similar large particles but showed obscure grain boundaries compared to those at -0.8 V, which was in accord with the above discussion that electrochemical intercalation of Na⁺ and/or K⁺ had occurred. As shown in Figure 6d, the electrolytically generated L₃Mo₆S₈ and LMo₃S₃ particles at -1.4 V were of nanometre sizes, which seemed to be poor in electric conductivity as the discharge phenomena were noticed under SEM. The poor conductivity of these particles should be unfavourable to their further electrochemical reduction, however, as discussed above, reactions (4) and (5) were slow in kinetics. These intermediates were further reduced to Mo at -1.6 V, the inset image in Figure 5e reveals nodular shapes of the generated Mo particles of 50 ~ 100 nm in size.

Constant cell voltage electrolysis was carried out between the MoS₂ pellet (1.45 g, 2 cm in diameter) cathode and the graphite rod anode to further understand the reduction mechanism of MoS₂ in the NaCl-KCl melt, as well as to make an initial process evaluation. By applying a cell voltage of 2.7 V, it was assumed that the thermodynamic and kinetic difficulties encountered in the reduction of the intermediates could be overcome, so that fast electrolysis can be implemented. Figure 7 shows the current response upon the application of the 2.7 V cell voltage, with the potential of the solid cathode monitored simultaneously, suggesting several reduction stages. These current changes can be referred to the XRD analyses (Figure 8) of the partially reduced products and the final product.

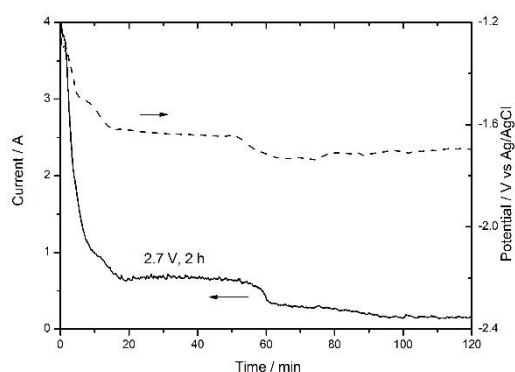


Figure 7. The current-time and cathode potential-time plots recorded during the constant cell voltage electrolysis of MoS₂ pellets (ca. 1.45g) at 2.7 V and 700 °C in the NaCl-KCl melt.

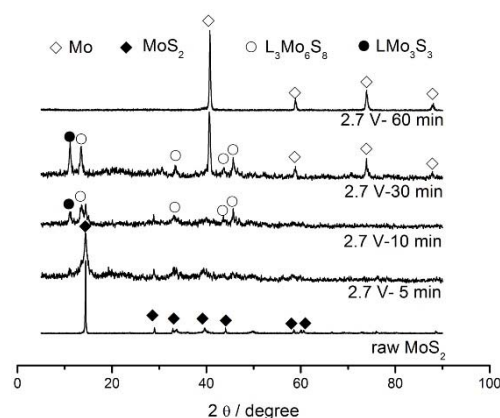


Figure 8. XRD patterns of the products from electrolysis of MoS₂ pellets (ca. 1.45 g) at the cell voltage of 2.7 V for different times in the NaCl-KCl melt at 700 °C.

The first stage lasted for about 5~8 min with the largest current, suggesting a very fast reaction. The XRD pattern of the 5-min product after washing in water showed amorphisation of the MoS₂ structure, apparently resulting from deintercalation of L during washing after electrochemical intercalation via reaction (1) as discussed above. The 10-min product consisted of mainly L₃Mo₆S₈ and LMo₃S₃, indicating that the second stage (~ 8~18 min) corresponded to reactions (2) and (3), which were still fast. The third stage between 18 and 60 min was relatively slow, and Mo became the dominant phase in the product, indicating most of the sulfide had been reduced. These analyses were in well agreement with the cathode potential-time plot as shown in Figure 7. The cathode potentials were around -1.3 V, -1.5 V and -1.65 V at the first, second and third stage, corresponding to the formation of L_xMoS₂, LMo₃S₃ and L₃Mo₆S₈, and metallic Mo respectively according to those results from the potentiostatic electrolysis.

The complete metallization of the whole cathode was accomplished within 2 hours, and the final product was nodular nanoparticles of Mo of 50~100 nm in size (Figure 6f). This kind of nano-Mo powder was stable during washing with water. The metal recovery reached about 94%, which is high considering the inevitable loss of nanoparticles during the washing, filtration and collection steps.

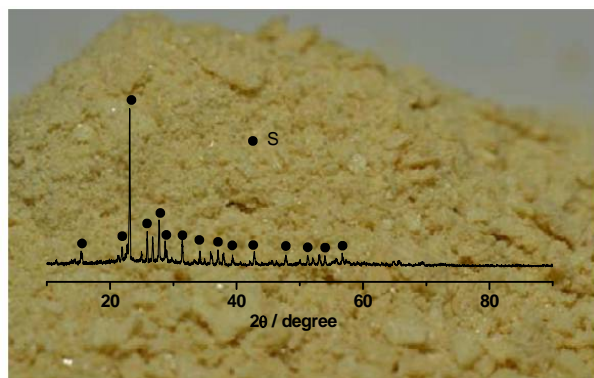


Figure 9. Photograph of the condensed anodic sulfur product with the XRD pattern inserted.

According to Figure 7, the current efficiency was as high as 92% for the 2 h electrolysis at 2.7 V (cell voltage), and the energy consumption was about 2.07 kWh/kg-Mo. Other important advantages of such solid metal sulfide electrolysis include: (1) the solubility of S^{2-} in the NaCl-KCl based melts can be very high (for example, 39 mol/L in NaCl at 712 °C),³² which allows fast diffusion and convection of S^{2-} ions from the cathode and then through the electrolyte to the anode;³³ (2) graphite is an ideal non-consumable anode material with sulfur as the product from anodic oxidation of S^{2-} , which has been evidenced not only by a previous study on solid WS_2 electrolysis,²⁷ but also by numerous works on electrolysis of dissolved metal sulfides.¹³⁻¹⁸ In this work, buff deposition was found on the water cooled top wall of the steel reactor, and collected and washed with water. The resultant yellow powder was identified by XRD to be element S as shown in Figure 9, confirming that the S^{2-} ions had been oxidised to S on the graphite anode.

Conclusions

Facile preparation of Mo nanopowder can be achieved through electrolysis of solid MoS_2 in NaCl-KCl at 700 °C. Studies from cyclic voltammetry, potentiostatic and constant cell voltage electrolysis together with XRD and EDX analyses, and SEM observation have shown that the MoS_2 phase was first reduced to L_xMoS_2 and $LMoS_2$ through continuous electrochemical insertion of Na^+ and/or K^+ . The next intermediate products were $L_3Mo_6S_8$ and LMo_3S_3 whose further reduction led to formation of the Mo nanopowder.

Compared to other steps, the reduction of $L_3Mo_6S_8$ and LMo_3S_3 was more difficult in kinetics, requiring a relatively higher overpotential for their quick reduction. Rapid electrolysis of MoS_2 has been realized at a cell voltage of 2.7 V with current efficiency as high as 92%. The electrolytic Mo nanopowders consisted of nodular nano-particles (50~100 nm in size) with high metal recovery. The anodic product was confirmed to be elemental sulfur. These findings can form the basis for the development of a new, fast, and environment friendly electrolytic process for the metallurgy of MoS_2 and the commercial production of nano-Mo powders.

Acknowledgements

This work received partial support from each of the NSFC (21173161, 20973130), the 863 project (2009AA03Z503), the MOE Program (NCET-11-0397), the Fundamental Research Funds for the Central Universities, the Large-scale Instrument and Equipment Sharing Foundation of Wuhan University, and the EPSRC (EP/J000582/1).

Notes and references

^a College of Chemistry and Molecular Sciences, Wuhan University, Wuhan, 430072, P. R. China

^b Department of Chemical and Environmental Engineering, and Energy and Sustainability Research Division, Faculty of Engineering, University of Nottingham, Nottingham, NG7 2RD, UK.

*Corresponding author. Tel & Fax +86 27 68756319

E-mail address: xbjin@whu.edu.cn (X. B. Jin)

- 1 M. Kutz, *Handbook of Materials Selection*, John Wiley & Sons, New York, 2002.
- 2 ASM Metals Handbook, *Properties and Selection: Irons, Steels and High-Performance Alloys*, ASM International, Materials Park, OH, 10th ed., 1990, vol. 1.
- 3 R. W. Revie, *Uhlig's Corrosion Handbook*, John Wiley & Sons, New York, 2nd ed., 2000.
- 4 R. Z. Zhu, X. Y. Lu, *Heat Resistant Steels and High Temperature Alloys*, Chemical Industry Press, Beijing, 1995 (in Chinese).
- 5 W. O. Winer, *Wear*, 1967, **10**, 422-452.
- 6 F. Z. Wang, D. C. Li, Y. Z. Sun, H. Wu. *Molybdenum materials and Their processing*, Metallurgical Industry Press, 2008 (in Chinese).
- 7 T. G. Xiang, *Molybdenum metallurgy*, Central South University Press, Changsha, 2009 (in Chinese).
- 8 H. L. Tu, G. Q. Zhao, Q. W. Guo, *Nonferrous Metals – Metallurgy, Material, Recovery and Environmental Protection*, Chemical Industry Press, 2002 (in Chinese).
- 9 C. S. Fu (Ed.), *Principles of Nonferrous Metallurgy*, Metallurgical Industry Press, 2nd ed., 2004 (in Chinese).
- 10 W. D. Xiao, Z. Q. Wu, *Removal and Recovery of Sulfur Dioxide*, Chemical Industry Press, 2001 (in Chinese).
- 11 A. F. Holleman, E. Wiberg, N. Wiberg. *Lehrbuch der Anorganischen Chemie*, Walter de Gruyter-Verlag, Berlin, New York, 91–100 ed., 1985, pp. 1096–1104.
- 12 P. M. Prasad, T. R. Mankhand, A. J. K. Prasad, *National Metallurgical Laboratory Technical Journal*, 1997, **39**, 39-58.
- 13 Y. Xiao, D. W. van der Plas, J. Bohte, S. C. Lans, A. van Sandwijk and M. A. Reuter, *J. Electrochem. Soc.*, 2007, **154**, D334-D338.
- 14 N. Q. Minh, N. P. Yao, *J. Electrochem. Soc.*, 1983, **130**, 1025-1029.
- 15 N. Q. Minh, R. O. Loutfy, N. P. Yao, *J. Electroanal. Chem. Interfacial Electrochem.*, 1982, 131. 229-242.
- 16 N. Q. Minh, R. O. Loutfy, N. P. Yao, *J. Appl. Electrochem.*, 1982, **12**, 653-658.
- 17 M. Skyllas, B. J. Welch, *Electrochim. Acta*, 1978, **23**, 1157 -1163.
- 18 D. J. Wang, *Yunnan Metallurgy*, 1995, **5**, 30-33(in Chinese).
- 19 G. Z. Chen, D. J. Fray, T. W. Farthing, *Nature*, 2000, **407**, 361-364.
- 20 S. Q. Jiao, L. L. Zhang, H. M. Zhu, D. J. Fray, *Electrochim. Acta*, 2010, **55**, 7016-7020.
- 21 X. L. Zou, X. G. Lu, Z. F. Zhou, C. H. Li, W. Z. Ding, *Electrochim. Acta*, 2011, **56**, 8430-8437.
- 22 A. M. Abdelkader, K. T. Kilby, A. Cox, D. J. Fray, *Chem. Rev.*, 2013, **113**, 2863-2886.
- 23 D. J. Fray, T. W. Farthing, G. Z. Chen, WO Pat., 9964638, 1999.
- 24 D. J. Fray, *JOM-J. Miner. Met. Mater. Soc.*, 2001, **53**, 26-31.
- 25 G. M. Li, D. H. Wang, X. B. Jin, G. Z. Chen, *Electrochem. Commun.*, 2007, **9**, 1951-1957.
- 26 X. L. Ge, X. D. Wang, S. Seetharaman, *Electrochim. Acta*, 2009, **54**, 4397-4402.
- 27 T. Wang, H. P. Gao, X. B. Jin, H. L. Chen, J. J. Peng, G. Z. Chen, *Electrochem. Commun.*, 2011, **13**, 1492-1495.
- 28 P. Gao, X. B. Jin, D. H. Wang, X. H. Hu, G. Z. Chen, *J. Electroanal. Chem.*, 2005, **579**, 321-328.
- 29 A. Zak, Y. Feldman, H. Cohen, V. Lyakhovitskaya, G. Leitius, R. Popovitz-Biro, S. Reich, R. Tenne, *J. Am. Chem. Soc.*, 2002, **124**, 4747-4758.
- 30 Y. Deng, D. H. Wang, W. Xiao, X. B. Jin, X. H. Hu, G. Z. Chen, *J. Phys. Chem. B*, 2005, **109**, 14043-14051.
- 31 W. Xiao, X. B. Jin, Y. Deng, D. H. Wang, X. H. Hu, G. Z. Chen, *ChemPhysChem*, 2006, **7**, 1750-1758.
- 32 N. Shivgulam, D. Barham, W. H. Rapso, Sodium chloride (and) potassium: their effects on kraft smelt, *Pulp Paper Can.*, 1978, **80**, 89-92
- 33 H. P. Gao, X. B. Jin, S. W. Zou, F. Z. Ling, J. J. Peng, Z. Y. Wang, G. Z. Chen, Liquid Diffusion of the Instantaneously Released Oxygen Ion in the Electrolytic Porous Fe from Solid Fe₂O₃ in Molten CaCl₂, *Electrochim. Acta*, 2013, **107**, 261-268.